General Relativistic Magnetohydrodynamic Simulations of Collapsars with Multipole Self-Gravity

Piotr Płonka[1] & Agnieszka Janiuk[1]

[1]Center for Theoretical Physics of the Polish Academy of Sciences

BLACK HOLES AT DIFFERENT FLAVOURS

Long Gamma-Ray Bursts

Long GRBs originate from **massive**, **rapidly rotating** stars collapsing into black holes and launching **relativistic jets**.

- Their association with star-forming galaxies points to short-lived, **massive stellar progenitors**.
- Long GRBs are associated with Type Ib/c supernovae from **stripped-envelope massive stars**.
- A newly formed **black hole–accretion-disk system** powers a **relativistic jet**.

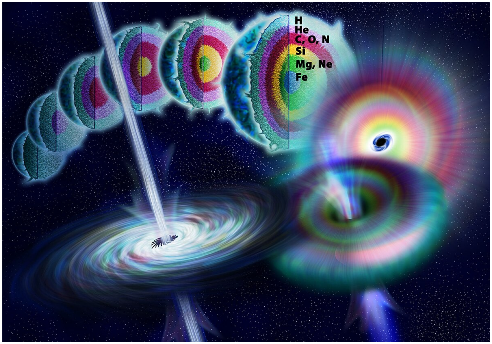

Figure 1: Schematic illustration of the collapsar engine: a relativistic jet emerging from a collapsing massive star.

Types of Collapsar GRMHD Simulations

Dynamical spacetime

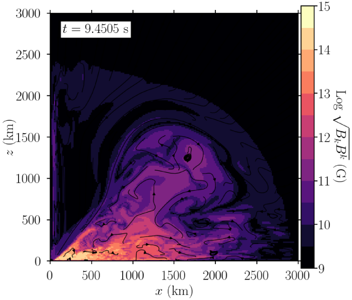

Shibata et al. (2025)

- Most self-consistent treatment of gravity
- Realistic microphysics
- Tracks BH formation
- Very expensive; typically axisymmetric

Fixed Kerr spacetime

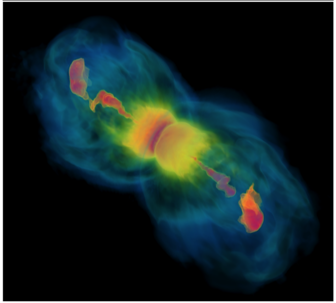

Gottlieb et al. (2022)

- Efficient; enables long 3D runs
- No self-gravity or BH evolution
- Requires a pre-existing BH

Evolving Kerr spacetime with self-gravity

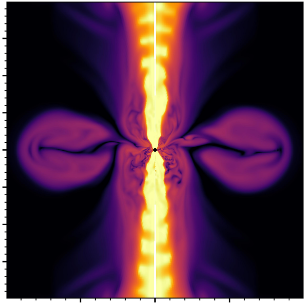

Płonka & Janiuk (2026)

- Efficient; enables long 3D runs
- Self-gravity + BH evolution
- Requires a pre-existing BH

FUGUE: GPU Implementation and Numerical Methods

Motivation for developing a new GPU-accelerated code

- **GPU acceleration** enables long-duration **three-dimensional GRMHD simulations**.
- Coupling **weak-field self-gravity** to **quasi-stationary Kerr black-hole evolution**.

- FUGUE is a conservative, **finite-volume**, **shock-capturing** code that solves the **ideal-GRMHD equations** in **Kerr spacetime**.
- The code is written in **CUDA C++** with **CUDA-aware MPI**.
- The code uses **PPM** reconstruction, the **HLLE** Riemann solver, and **RK2** time integration.
- **Flux-constrained transport** maintains the discrete $\nabla \cdot \boldsymbol{B} = 0$ constraint to round-off accuracy.
- Optional modules provide **Kerr metric updates** and **weak-field multipole self-gravity**.

General Relativistic Magnetohydrodynamics (GRMHD)

- The code solves the covariant equations of ideal GRMHD: the **continuity equation**, the **conservation of energy–momentum**, and the **induction equation**:

$$\nabla_\mu \left(\rho u^\mu\right) = 0, \quad \nabla_\mu T^{\mu\nu} = 0, \quad \nabla_\mu \left({}^*F^{\mu\nu}\right) = 0. \tag{1}$$

- The total **stress–energy tensor** is the sum of the **fluid** and **electromagnetic** parts:

$$T^{\mu\nu}_{MHD} = (\rho + u + p + b^2)u^\mu u^\nu + \left(p + \frac{b^2}{2}\right) g^{\mu\nu} - b^\mu b^\nu. \tag{2}$$

- In **ideal MHD**, the **electric field vanishes** in the comoving frame:

$$u_\nu F^{\mu\nu} = 0, \quad u_\mu b^\mu = 0. \tag{3}$$

FUGUE: Special Relativistic Hydrodynamics (SRHD)

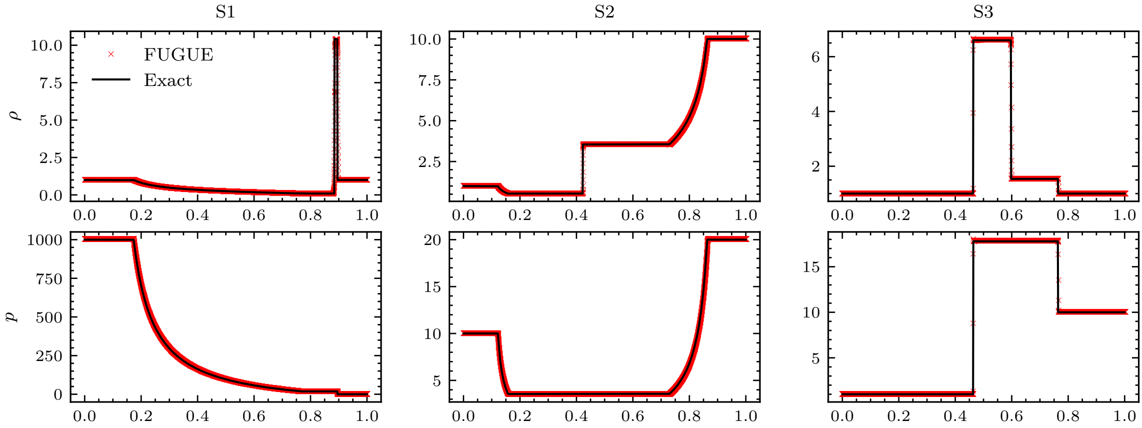

Figure 2: Relativistic hydrodynamic shock-tube tests S1–S3. The figure compares the FUGUE results with the exact solutions. The calculations use PPM reconstruction at a resolution of $N = 8192$.

FUGUE: Special Relativistic Magnetohydrodynamics (SRMHD)

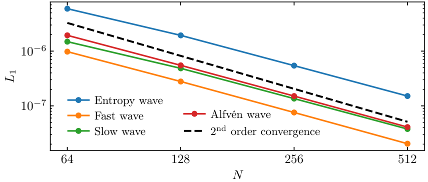

Figure 3: Linear-wave convergence; the dashed line marks second order.

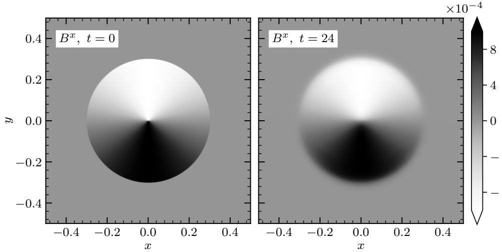

Figure 4: Magnetic-loop advection from $t = 0$ to $t = 24$.

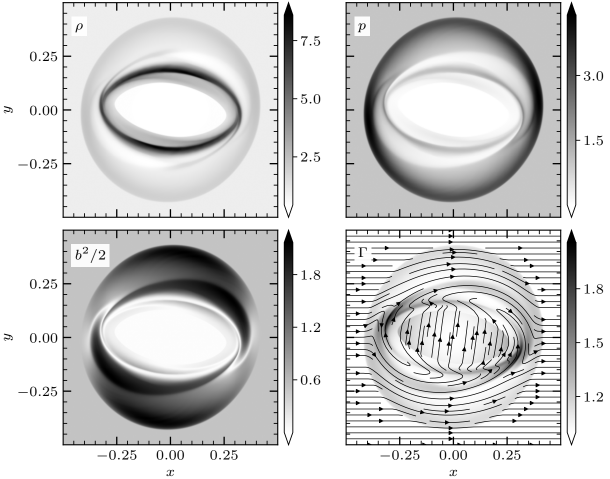

Figure 5: Relativistic magnetic-rotor test at final time.

FUGUE: General Relativistic Magnetohydrodynamics (GRMHD)

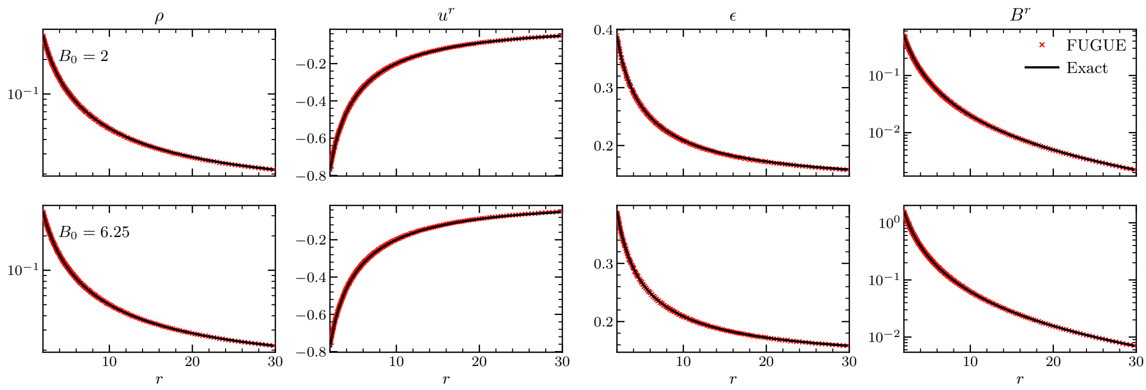

Figure 6: Magnetized Bondi–Michel accretion in Schwarzschild spacetime for two magnetic-field strengths, $B_0 = 2$ and $B_0 = 6.25$. The panels compare the FUGUE radial profiles of ρ, u^r, ϵ, and B^r with the exact solutions, confirming a steady spherical accretion flow.

FUGUE: General Relativistic Magnetohydrodynamics (GRMHD)

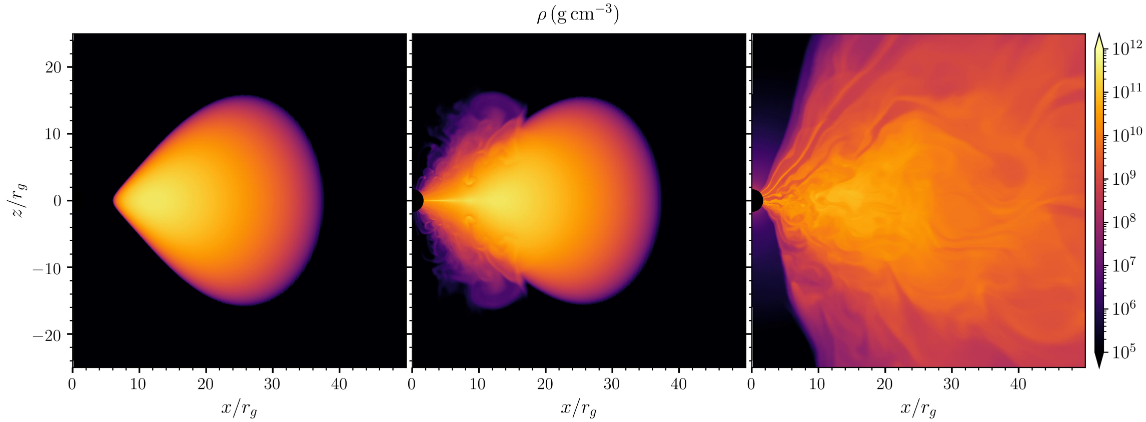

Figure 7: Rest-mass density evolution of the magnetized Fishbone–Moncrief torus at $t = 0$, 250, and $2000\,t_g$, from left to right. The model uses $M_{BH} = 3\,M_\odot$, $a_* = 0.8$, $r_{in} = 6\,r_g$, $r_{max} = 12\,r_g$, $\beta = 50$, and a resolution of 1024×1024.

FUGUE: Quasi-Stationary Kerr Black-Hole Evolution

- The code includes **quasi-stationary evolution** of the central **Kerr black-hole mass and dimensional spin parameter** a (with $a_* = a/M_{BH}$):

$$\frac{da}{dt} = \frac{\dot{J}}{M_{BH}} - \frac{a}{M_{BH}}\dot{E}. \tag{4}$$

- The **angular-momentum** and **energy fluxes** are computed at the inner boundary:

$$\dot{J} = -\int d\theta d\phi \, \sqrt{-g}\, T^r{}_\phi, \qquad \dot{E} = \int d\theta d\phi \, \sqrt{-g}\, T^r{}_t. \tag{5}$$

- The black-hole mass evolves according to:

$$\frac{dM_{BH}}{dt} = \dot{E}. \tag{6}$$

- The evolving Kerr metric adds an **energy source term**:

$$S_t = \frac{1}{2}\sqrt{-g}\, T^{\mu\nu}\, \partial_t g_{\mu\nu}, \qquad \partial_t g_{\mu\nu} = \frac{\partial g_{\mu\nu}}{\partial M_{BH}}\dot{M}_{BH} + \frac{\partial g_{\mu\nu}}{\partial a}\dot{a}. \tag{7}$$

FUGUE: Weak-Field Multipole Self-Gravity

- The code includes an optional **effective weak-field self-gravity module**, valid for:

$$|\Phi| \ll 1. \tag{8}$$

- The gravitational potential is obtained from a **Poisson equation**:

$$\nabla^2\Phi = 4\pi\varrho, \qquad \varrho = E + S = (\rho + u + p + b^2)(2\Gamma^2 - 1) + 2p - 2(b^\mu n_\mu)^2 \tag{9}$$

- The effective density is decomposed into **spherical harmonics**:

$$\varrho_{\ell m}(r) = \int \varrho(r,\theta,\phi) Y^*_{\ell m}(\theta,\phi)\, d\Omega, \qquad \Phi = \sum_{\ell=0}^{\ell_{\max}} \sum_{m=-\ell}^{\ell} \Phi_{\ell m}(r) Y_{\ell m}(\theta,\phi). \tag{10}$$

- Self-gravity couples to the GRMHD equations through a **four-force** orthogonal to the fluid four-velocity:

$$\nabla_\mu T^{\mu\nu} = G^\nu, \quad G^\mu = -\left[(\rho + u + p + b^2)\,(g^{\mu\nu} + u^\mu u^\nu) - b^\mu b^\nu\right] \nabla_\nu \Phi, \quad u_\mu G^\mu = 0. \tag{11}$$

FUGUE: Weak-Field Multipole Self-Gravity

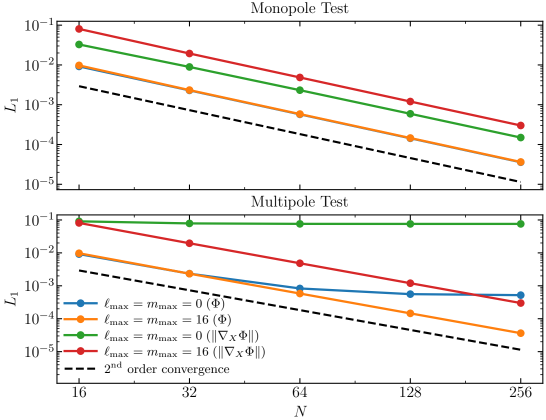

Figure 8: Relative L_1 errors in the self-gravity Poisson solver. The panels show the gravitational potential Φ and its gradient $\|\nabla_X \Phi\|$; dashed lines indicate second-order convergence.

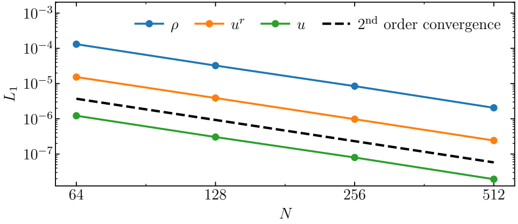

Figure 9: Convergence test for a self-gravitating polytropic star. The model preserves hydrostatic equilibrium, while the L_1 errors of the primitive variables decrease at second order.

$$\frac{dp}{dr} = -\rho \frac{d\Phi}{dr}. \tag{12}$$

Hydrostatic equilibrium

FUGUE: Toomre-Unstable Disk around a Kerr Black Hole

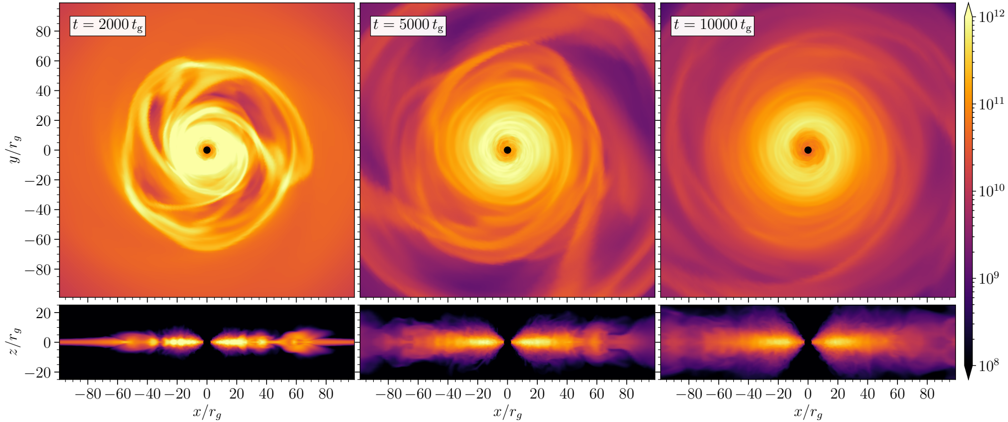

Figure 10: Density maps, $\rho\,(g\,cm^{-3})$, for a self-gravitating, Toomre-unstable disk. They show the growth of non-axisymmetric structure, beginning near the black hole and subsequently extending outward. At $\ell_{\max} = m_{\max} = 16$, global modes are captured, whereas local fragmentation remains unresolved.

- In the **standard GRMHD configuration**, FUGUE achieves throughput **comparable to the fastest published GPU-accelerated GRMHD codes**.

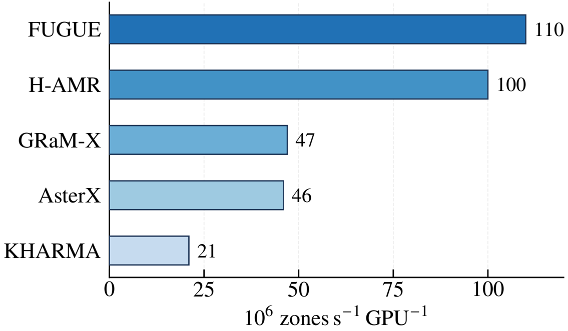

Figure 11: Indicative single-GPU throughput of GRMHD codes. The published benchmark configurations are not identical.

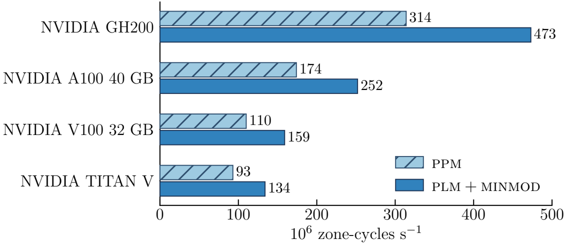

Figure 12: Zone-cycle performance for different NVIDIA GPUs. The benchmark uses a 256^3 Fishbone–Moncrief torus with PPM reconstruction and RK2 time integration.

Collapsars with Multipole Self-Gravity

- We investigate how the **internal structure of the progenitor** and **self-gravity** affect the evolution of collapsar systems, and their consequences for **black-hole evolution**.

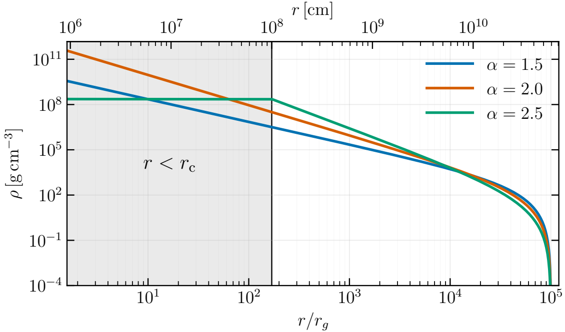

Figure 13: Initial density profiles for a $30\,M_\odot$ collapsar with $M_{BH} = 4\,M_\odot$, with three density slopes: $\alpha = 1.5$, 2.0, and 2.5.

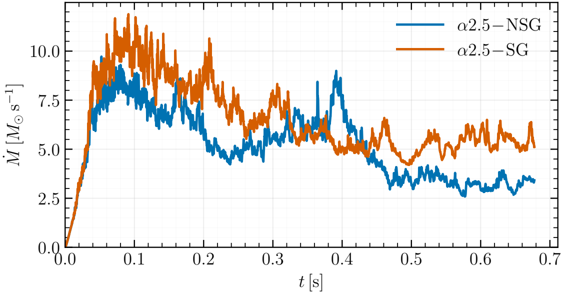

Figure 14: Mass accretion rate for the models with self-gravity is higher due to shorter dynamical timescale.

- FUGUE enables us to follow the **black-hole spin evolution** during accretion and **jet launching**. Including **self-gravity** leads to a **faster spin-down** of the black hole.

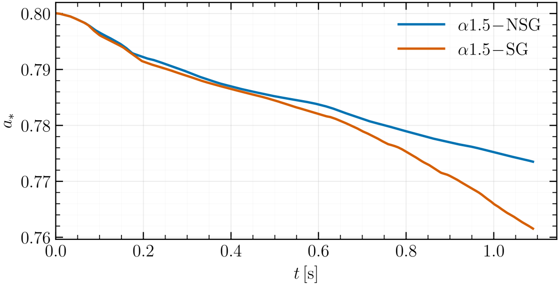

Figure 15: Spin evolution in collapsar with $\alpha = 1.5$.

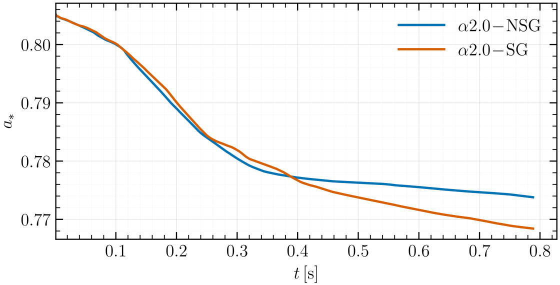

Figure 16: Spin evolution in collapsar with $\alpha = 2.0$.

Black-Hole Formation and Collapsar Evolution

- We investigate the **formation of black holes** from two pre-collapse progenitors using `GR1D`, and then **remap the post-collapse profiles into FUGUE** to study their evolution.

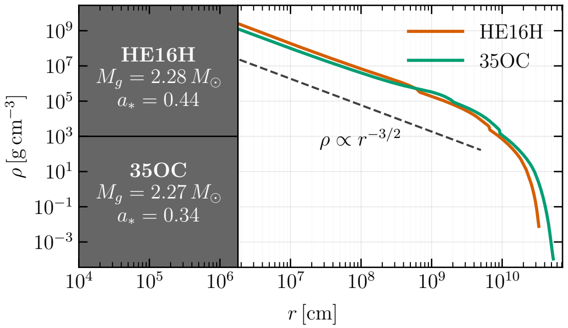

Figure 17: Density profiles of the **HE16H** and **35OC** progenitors after collapse. The shaded region marks the material associated with the newly formed black hole.

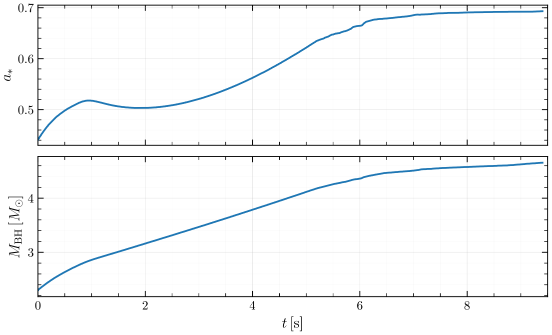

Figure 18: Evolution of the dimensionless black-hole spin a_* and black-hole mass M_{BH} after black-hole formation.

Conclusions

- We introduced **FUGUE** (submitted to ApJS), a new GPU-accelerated GRMHD code, including optional **black-hole evolution** and **weak-field multipole self-gravity**
- The **multipole self-gravity** module captures **gravitational instabilities**.
- Including **self-gravity** modifies the collapsar evolution: it shortens the dynamical timescale, enhances **mass accretion**, and changes the **black-hole mass and spin evolution**

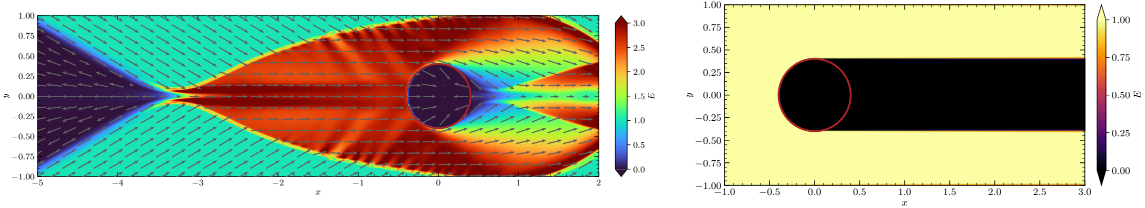

Figure 19: M1 neutrino transport tests as a step toward including more realistic **microphysics** in collapsar simulations.

Thank You for Your Attention!

This work was partially supported by the National Science Centre, Poland, under grant No. 2023/50/A/ST9/00527. We acknowledge the PLGrid infrastructure and ACK Cyfronet AGH for computing resources under grant No. PLG/2026/019543.

(A&A 709, A80)